# Assessment of the Energy Balance Closure under Advective Conditions and Its Impact Using Remote Sensing Data

ZIWEI XU

*State Key Laboratory of Earth Surface Processes and Resource Ecology, Faculty of Geographical Science, Beijing Normal University, Beijing, China*

YANFEI MA

*Department of Geography, Handan College, Hebei, China*

SHAOMIN LIU

*State Key Laboratory of Earth Surface Processes and Resource Ecology, Faculty of Geographical Science, Beijing Normal University, Beijing, China*

WENJIAO SHI

*Key Laboratory of Land Surface Pattern and Simulation, Institute of Geographic Sciences and Natural Resources Research, Chinese Academy of Sciences. and College of Resources and Environment, University of Chinese Academy of Sciences, Beijing, China*

JIEMIN WANG

*Cold and Arid Regions Environmental and Engineering Research Institute, Chinese Academy of Sciences, Lanzhou, China*

(Manuscript received 25 February 2016, in final form 28 September 2016)

ABSTRACT

A unique and intensive flux observation matrix was established during May to September of 2012 in an oasis–desert area located in the middle reaches of the Heihe River basin, China. The flux observation matrix included 22 eddy covariance systems belonging to the first thematic experiment of the Heihe Watershed Allied Telemetry Experimental Research (HiWATER) project. The energy balance closure ratio (EBR) was assessed and possible mechanisms were investigated using remote sensing data. The results showed that 1) the EBR was in the range of 0.78–1.04 at all sites with an average EBR of 0.92, and 2) the calculated daily EBR exhibited better performance than the 30-min averages. 3) The heat storage cannot be ignored during the crop growing season. An improvement of approximately 6% in the total closure was found after considering the heat storage terms (canopy and photosynthesis storage) in the energy budget at the maize surface, and the canopy and photosynthesis showed approximately equal contributions of 3% for each storage term. The results also showed that 4) the land heterogeneous surface had a significant effect on the EBR. The EBR decreased with land surface heterogeneity increasing (taking the standard deviation of the surface temperature in the eddy covariance system source area as an index). The EBR also decreased when irrigation occurred and increased after irrigation was completed. The advection or secondary circulation broke the closed system of the energy balance given the phenomenon of EBR increasing when the advection or secondary circulation occurred.

## 1. Introduction

The eddy covariance system (EC) is widely used to measure surface energy fluxes around the world, and it has become a standard tool in the study of land surface–atmosphere boundary layer interactions (Aubinet et al. 2012). The EC method is also used as the main technique in the global Flux Network (FLUXNET) of micrometeorological measurement sites that monitors terrestrial carbon, water, and energy cycles (Aubinet et al. 2000). These measurements are taken as ground truth values to validate land surface model results or remote sensing estimations (Xu et al. 2011; Bai et al. 2015). However, the EC measurements

*Corresponding author e-mail*: Dr. Ziwei Xu, xuzw@bnu.edu.cn; Wenjiao Shi, shiwj@lreis.ac.cn

DOI: 10.1175/JAMC-D-16-0096.1

are subject to several limitations, especially problems related to the energy imbalance. Nevertheless, the energy balance equation is commonly used in land surface or remote sensing models. Therefore, the energy imbalance has a significant influence on calibration and validation of models, and this imbalance has implications for how these estimates should be compared with model simulations (Twine et al. 2000; Jia et al. 2012).

The energy balance closure is the concept that the sum of sensible and latent heat fluxes from EC is not equal to or less than the available energy under various surfaces, and several reasons for the energy imbalance have been summarized by previous researchers (Wilson et al. 2002; Foken 2008; Cava et al. 2008; Foken et al. 2011). Generally, the underlying cause of the imbalance was attributed to measurement errors, not fully considering the storage term, mismatch between the scales of the energy balance components, and large-eddy transport or secondary circulations that were not captured by EC. Foken (2008) concluded that mesoscale circulations resulting from landscape heterogeneity are likely responsible for the energy imbalance at the tower measurement level. Stoy et al. (2013) investigated the relationship between energy balance closures and landscape heterogeneity across 173 ecosystems in the FLUXNET, and found that landscape-level heterogeneity cannot be ignored in the incomplete energy balance closure ratio (EBR). However, the exact factors leading to the imbalance are still under debate. Generally, an imbalance of approximately 10%–30% has been traditionally reported (Wilson et al. 2002; Foken 2008; Franssen et al. 2010; Kawai and Kanda 2010; Liu et al. 2013). An average EBR of 0.84 (ranging from 0.34 to 1.69) was reported in an evaluation of 22 sites (50 site years) in the FLUXNET (Wilson et al. 2002). The EBR was studied at a FLUXNET boreal forest site in Finland, and an average EBR of 0.72 was found (Sánchez et al. 2010). However, the EBR was improved to 0.94 after filtering the data according to small friction velocity, stability and neutral conditions, and unfavorable wind direction. The Energy Balance Experiment (EBEX-2000) was designed to specifically study the causes of the energy imbalance, and an energy deficit of 10% was still observed after considering all the possible influences (Oncley et al. 2007). The Chinese Terrestrial Ecosystem Flux Research Network (ChinaFLUX) is a long-term network of flux observation sites. An average imbalance of approximately 27% was reported using ChinaFLUX data (Li et al. 2005). The surface energy balance closures in typical surfaces over the Heihe River basin (HRB) of China ranged from 0.79 to 0.89 (Liu et al. 2011); these data came from the Watershed Allied Telemetry Experimental Research (WATER) project. The Multiscale Observation Experiment on Evapotranspiration of Heihe Watershed Allied Telemetry Experimental Research (HiWATER-MUSOEXE) was conducted in the middle reaches of the HRB in May through September of 2012 and involved a flux observation matrix (Li et al. 2013; Xu et al. 2013). One primary objective of the HiWATER-MUSOEXE was to investigate the underlying reason for the energy imbalance.

The objectives of this study are 1) to assess the EBR using the intensive flux observation matrix (22 EC sets) under advective conditions and 2) to identify the possible causes of the energy imbalance.

## 2. Experiment and methods

### *a. Flux observation matrix in HiWATER-MUSOEXE*

During HiWATER-MUSOEXE, a unique and intensive flux observation matrix was established. The matrix was composed of two nested experimental areas, a large experimental area (oasis–desert area) with a scope of 30 km × 30 km, and a kernel experimental area (within oasis) with a scope of 5.5 km × 5.5 km (Fig. 1). The large experimental area was located in an oasis–desert area with primary underlying surfaces of cropland, sandy desert, desert steppe, Gobi Desert, wetland, and residential areas. One superstation (38°51′20″N, 100°22′20″E) and four ordinary stations were located in the large experimental area, and the 17 sites in the kernel experimental area were divided according to the distribution of land cover/use, windbreak, residential area, soil moisture, and irrigation status. Overall, 22 EC sets observations (site 15 is a superstation equipped with two levels of ECs) were used in this study. The sonic anemometers of the ECs were aimed toward the north and were installed at a height of approximately 3–7 m, except for an EC with a height of 34 m in the upper layer of the superstation. Five EC combinations were used in the matrices, namely, CSAT3 and Li7500 (sites 2, 5, 8, 10, 11, 12, and 14 and the Batman Gobi site, Shenshawo desert site, and Huazhaizi desert steppe site), CSAT3 and Li7500A (sites 4, 6, 7, 13, and 15), CSAT3 and EC150 (site 17), Gill and Li7500 (site 16), and Gill and Li7500A (sites 1, 3, and 9 and the Zhangye wetland site). The installation locations of the ECs included several surfaces, that is, maize cropland, vegetable cropland, orchard, residential area, Gobi Desert, sandy desert, desert steppe, and wetland, which are the typical surfaces in western China. One automatic weather station (AWS) was also installed at each site and was equipped with sensors that can record wind speed and direction, air temperature and humidity, soil temperature and moisture profile, four-component radiation, air pressure, precipitation, soil heat flux, and infrared temperature. To monitor the canopy heat storage, two layers of air temperature and humidity sensors were added to sites 7

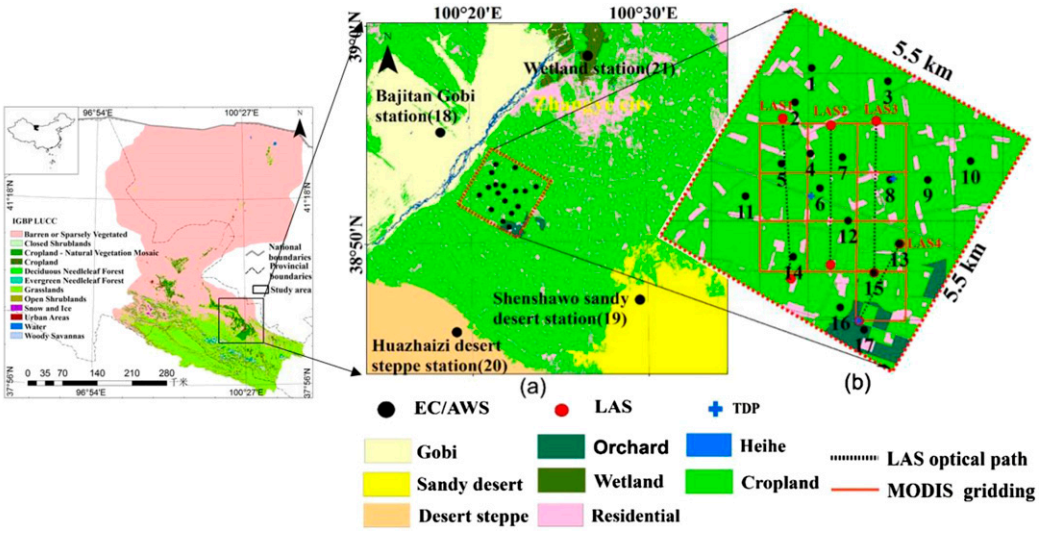


FIG. 1. Spatial locations of the 21 study sites over two nested experimental areas during the HiWATER-MUSOEXE research period.

and 12 on 19 July, site 15 on 15 July, and site 17 on 6 August 2012. The biomass was also observed at each site (Wang et al. 2012). During the experiment, four large-aperture scintillometer (LAS) groups were installed in the $3 \times 3$ and $2 \times 1$ MODIS pixels within the kernel experimental area to measure the area averaged sensible heat flux; the transpiration of shelterbelts with different heights and diameters at breast height was measured using a thermal dissipation probe near sites 6, 8, and 17 (Fig. 1). Details can be found in Liu et al. (2016).

### b. *Data processing*

The Edire (http://www.geos.ed.ac.uk/abs/research/micromet/EdiRe/) and Eddypro (http://www.licor.com/env/products/eddy_covariance/software.html) software packages were used to process the EC data, which were developed by the University of Edinburgh and LI-COR Biosciences (Lincoln, Nebraska), respectively. Data processing procedures included spike detection, lag correction of $H_2O/CO_2$ relative to the vertical wind component, coordinate rotation (2D rotation), sonic virtual temperature correction, frequency response correction and density fluctuation. In addition, the EC systems with a Gill-WindMaster (Lymington, United Kingdom) sonic anemometer were used the angle of attack error correction. The EC data were averaged over 30-min periods. Data quality assessment was performed for turbulent flux in each 30-min run with the indices 0, 1, and 2 representing high- (class 1), medium- (class 2), and low-quality (class 3) data (Mauder and Foken 2004), respectively. Classes 1 and 2 were selected for analysis. In addition, the 30-min flux data were further screened, including 1) rejection of data associated with sensor malfunction, 2) rejection of data within 1 h of precipitation, 3) rejection of incomplete 30-min raw data, and 4) rejection of data because of a friction velocity $u_*$ of less than $0.1\,\mathrm{m\,s^{-1}}$ ($0.12\,\mathrm{m\,s^{-1}}$ for the upper EC at site 15) at night. When calculating the accumulative evapotranspiration, the nonlinear regression method was used to interpolate the missing data (Berbigier et al. 2001).

The AWS data were checked for diurnal variation, and data that were clearly beyond the range of physical possibility were rejected. Finally, the data were averaged to 30-min periods.

In addition to the ground measurement data, the remote sensing data were processed as follows. Nine Advanced Spaceborne Thermal Emission and Reflection Radiometer (ASTER; http://asterweb.jpl.nasa.gov/) images were acquired from May to September 2012, namely, 15 June, 24 June, 10 July, 2 August, 11 August, 18 August, 27 August, 3 September, and 14 September. These images covered almost the entire growth period of maize. The resolution of thermal infrared bands was 90 m and was atmospherically corrected. The overpassing times for these images were approximately 1212–1219 Beijing standard time (BST; the local solar noon is 1318). The land surface temperature (LST) was retrieved from the thermal infrared bands using the split-window algorithm (Zhou et al. 2015). The land-cover data were generated based on high-spatial-resolution Huan Jing-1 (HJ-1) charge-coupled-device images via supervised classification (Ma et al. 2015). One airborne Thermal Airborne Spectrographic

Imager (TASI) image was used. The TASI image was acquired by the TASI-600 push-broom hyperspectral thermal sensor system during 1045–1510 BST on 7 July 2012. The resolution of the TASI image was 3 m.

### c. Methods

#### 1) Energy balance closure

The equation used to calculate the EBR is defined as follows:

$$\mathrm{EBR} = \frac{\sum(H + \mathrm{LE})}{\sum(R_n - G_0 - S)}, \tag{1}$$

where $H$ and LE are the sensible and latent heat flux, respectively; $R_n$ is the net radiation; $G_0$ is the surface soil heat flux; and $S$ is the storage term. The method used to evaluate the closure of the EC was the cumulative sum of $R_n - G_0 - S$ and $H + \mathrm{LE}$ over specified time periods, for example, over a crop growing season or an entire year.

Energy balance closure can also be evaluated using the ordinary least squares (OLSs) method, which was established the relationships between the 30-min flux ($H$ + LE) and the available energy ($R_n$ − $G_0$). The linear regression coefficients (slope and intercept) could be derived from the OLSs, and the ideal closure has an intercept of 0 and a slope of 1.

#### 2) Storage terms

The ''PlateCal'' approach was used to calculate the surface soil heat flux $G_0$ (Liebethal et al. 2005):

$$G_0 = G_{\mathrm{obs}} + \int_0^{z_r} \frac{\partial \rho_s c_s T(z)}{\partial t} dz, \tag{2}$$

where $G_{\mathrm{obs}}$ is the soil heat plate measurement, $t$ is time, $z_r$ is the depth of the soil plate, $z$ is the depth below the soil surface, and $T$ is the soil temperature. The volumetric heat capacity ($\rho_s c_s$) was calculated from the soil water content, soil porosity, and the heat capacity of dry soil and liquid water (Yang and Wang 2008).

For the canopy, the storage $S_c$ was calculated as follows (Meyers and Hollinger 2004):

$$S_c = \frac{\Delta\theta(m_w c_w + m_b c_b)}{\Delta t}, \tag{3}$$

where $\Delta\theta$ is the change of air temperature within the canopy; $\Delta t$ is the time interval; $m_w$ and $m_b$ are the measured mass of water and biomass, respectively; and $c_w$ and $c_b$ are the specific heat capacities for plant water and biomass, respectively (Jacobs et al. 2008).

The photosynthesis storage was calculated from the following procedures. The net ecosystem exchange of carbon dioxide ($CO_2$) (NEE) can be represented as follows (Jacobs et al. 2003):

$$\mathrm{NEE} = A_n + R_s, \tag{4}$$

where $A_n$ is the assimilation flux (converting to photosynthesis flux $S_p$ by a factor) and $R_s$ is soil and plant respiration. The NEE was obtained from EC, and $R_s$ was calculated using the simple model of Fang and Moncrieff (2001). The factor of energy flux measured from EC converting to the photosynthesis rate $S_p$ was adopted by Meyers and Hollinger (2004).

#### 3) Remote sensing model

In this study, the surface energy balance system (SEBS) developed by Su (2002) was used to estimate the turbulent heat flux. In the SEBS model, computations of the sensible and latent heat fluxes are constrained by considering the dry-limit and wet-limit conditions. Under the dry limitation, the latent heat flux (LE) is set to zero due to the limitation of soil moisture and the sensible heat flux $H_{\mathrm{dry}}$ is at the maximum value. Under the wet limitation, evaporation occurs for the potential rate of $\mathrm{LE}_{\mathrm{wet}}$, and the minimum sensible heat flux $H_{\mathrm{wet}}$ can be calculated by the reversed Penman–Monteith equation assuming that the surface resistance is zero. Under given surface temperatures and meteorological conditions at the reference height, the sensible heat flux $H$ is computed on the basis of the Monin–Obukhov similarity theory:

$$H = k u_* \rho C_p (\theta_0 - \theta_a)\left[\ln\left(\frac{z-d}{z_{0\mathrm{m}}}\right) - \psi_h\left(\frac{z-d}{L}\right) + \psi_h\left(\frac{z_{0\mathrm{h}}}{L}\right)\right]^{-1}, \tag{5}$$

where $z$ is the height above the surface; $u$ is the wind speed; $u_*$ is the friction velocity; $\rho$ is the density of air; $C_p$ is the specific heat for air at constant pressure; $k$ is the von Kármán constant; $d$ is the zero plane displacement height; $z_{0\mathrm{m}}$ and $z_{0\mathrm{h}}$ are the roughness heights for momentum and heat transfer, respectively; $\theta_0$ is the potential temperature at the surface; $\theta_a$ is the potential air temperature at height $z$; $\psi_m$ and $\psi_h$ is the stability correction function for momentum and sensible heat transfer, respectively; and $L$ is the Obukhov length.

The relative evaporative fraction ($\mathrm{EF}_r$) and evaporative fraction (EF) can then be expressed as

$$\mathrm{EF}_r = \frac{H_{\mathrm{dry}} - H}{H_{\mathrm{dry}} - H_{\mathrm{wet}}} \quad \text{and} \quad \mathrm{EF} = \frac{\mathrm{EF}_r \times \mathrm{LE}_{\mathrm{wet}}}{R_n - G_0}. \tag{6}$$

TABLE 1. Energy balance closure at each site (June–September 2012). GB is the Bajitan Gobi station; SSW is the Shenshawo sandy desert station; HZZ is the Huazhaizi desert steppe station; WL is the Zhangye wetland station.

| Site | EBR | EBR_OLR | Slope | Intercept | $R^2$ | $n$ | Land cover |
|---|---|---|---|---|---|---|---|
| 1 | 1.01 | 0.96 | 0.88 | 33.85 | 0.90 | 2072 | Vegetable |
| 2 | 0.90 | 0.88 | 0.84 | 14.95 | 0.94 | 2328 | Maize |
| 3 | 0.94 | 0.91 | 0.88 | 15.52 | 0.92 | 2472 | Maize |
| 4 | 0.84 | 0.80 | 0.71 | 27.67 | 0.80 | 2113 | Residential area |
| 5 | 0.82 | 0.78 | 0.73 | 26.26 | 0.92 | 2077 | Maize |
| 6 | 1.02 | 0.97 | 0.90 | 29.52 | 0.90 | 2166 | Maize |
| 7 | 0.93 | 0.89 | 0.82 | 28.13 | 0.89 | 2272 | Maize |
| 8 | 0.88 | 0.83 | 0.78 | 22.27 | 0.85 | 2103 | Maize |
| 9 | 0.81 | 0.79 | 0.75 | 18.11 | 0.91 | 2000 | Maize |
| 10 | 0.94 | 0.90 | 0.85 | 26.30 | 0.93 | 1971 | Maize |
| 11 | 0.92 | 0.88 | 0.83 | 23.50 | 0.92 | 2276 | Maize |
| 12 | 0.90 | 0.86 | 0.80 | 30.49 | 0.91 | 2250 | Maize |
| 13 | 0.99 | 0.95 | 0.90 | 24.88 | 0.87 | 2129 | Maize |
| 14 | 1.04 | 1.00 | 0.95 | 25.7 | 0.92 | 2164 | Maize |
| 15 lower level | 0.89 | 0.84 | 0.78 | 29.65 | 0.90 | 2326 | Maize |
| 15 upper level | 1.03 | 0.94 | 0.86 | 40.83 | 0.86 | 1382 | Maize |
| 16 | 0.93 | 0.81 | 0.70 | 50.71 | 0.70 | 1522 | Maize |
| 17 | 0.78 | 0.76 | 0.73 | 16.48 | 0.87 | 2001 | Orchard |
| GB | 0.90 | 0.82 | 0.72 | 30.72 | 0.82 | 1253 | Gobi Desert |
| SSW | 0.81 | 0.71 | 0.59 | 37.45 | 0.78 | 1493 | Sandy desert |
| HZZ | 1.01 | 0.99 | 0.97 | 6.59 | 0.93 | 1330 | Desert steppe |
| WL | 1.03 | 1.00 | 1.05 | −5.29 | 0.92 | 1932 | Wetland |
| Avg | 0.92 | 0.88 | 0.82 | 25.20 | 0.88 | 1983 | — |

The LE (or the evapotranspiration ET) is estimated based on closing the surface energy balance as follows:

$$\mathrm{LE} = \mathrm{EF} \times (R_n - G_0) = \frac{\mathrm{EF}_r \times \mathrm{LE}_{\mathrm{wet}}}{R_n - G_0} \times (R_n - G_0) = \mathrm{EF}_r \times \mathrm{LE}_{\mathrm{wet}}. \quad (7)$$

Further details regarding the SEBS model can be found in Su (2002) and the details of the parameterization schemes of $z_{0m}$, $z_{0h}$, and $G_0$ were reported in Ma et al. (2015). To obtain the daily ET, the constant solar radiation ratio method was used to be upscale to daily time scales (Xu et al. 2015).

#### 4) FOOTPRINT MODEL

The method proposed by Kormann and Meixner (2001), which is an Eulerian analytic flux footprint model, was used to obtain the flux footprint of the EC observations. The flux contribution of the chosen total source area was set to 95% for every 30-min flux datum.

## 3. Results and discussion

### *a. Assessment of energy balance closure*

We used two methods to assess the energy balance closure: the overall calculations according to Eq. (1) (EBR) and the ordinary linear regression (EBR_OLR) coefficients. For comparison, both methods were used to calculate the energy balance closure (Table 1). In Table 1, the soil heat storage was considered; however, the other storage items (i.e., canopy storage and photosynthesis storage) were not considered because of data limitations. All sites had a relatively high EBR. The EBR values were within the range of 0.78–1.04, and the results of the OLR calculations were within the range of 0.71–1.00. The ratio of the total turbulent heat flux to the total available energy for all sites was 0.92. The EBR in this study was similar to or slightly higher than the results of previous studies, for example, the EBR was 0.77 in the Kursk (Russia) experiment in 1988 (KUREX-88) for a cropland surface (Tsvang et al. 1991); 0.9–1.0 in the 1989 intensive field campaign of the First ISLSCP Field Experiment (FIFE-89) for grassland surface (Kanemasu et al. 1992); 0.62 in KUREX-91 for cropland surface (Panin et al. 1998); 0.86 in the 1998 Lindenberg Inhomogeneous Terrain–Fluxes between Atmosphere and Surface (LITFASS-98) for a bare soil surface (Beyrich et al. 2002); 0.7–0.8 in LITFASS-2003 for a cropland surface (Mauder et al. 2006); 0.9 in EBEX for a cotton crop surface (Oncley et al. 2007); 0.34–1.69 (averaged 0.84) in FLUXNET for several surfaces (Wilson et al. 2002); 0.58–1 in ChinaFLUX for several surfaces (Li et al. 2005); 0.78–0.91 over the Hai River basin under forest and cropland surfaces (Liu et al. 2013); and 0.79–0.87 in the Heihe River basin for cropland, forest, and grassland surfaces (Liu et al. 2011).

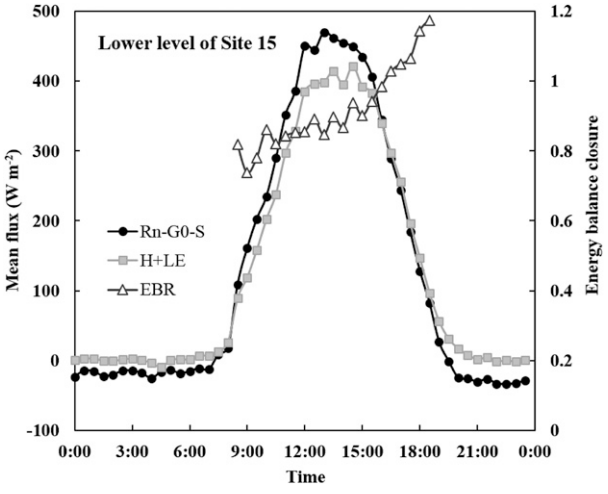


FIG. 2. Mean diurnal values of $R_n - G_0 - S$ (black circles), $H$ + LE (gray squares), and EBR (black open triangles; right $y$ axis) at the lower level of site 15 (EBR: 0830–1830, 16 Jul–15 Sep 2012).

### 1) THE DIURNAL COURSE OF EBR

Data from the typical site (lower level of the superstation) were selected to compute the diurnal course of the EBR. Figure 2 shows the diurnal variation of the EBR, the mean value of $R_n - G_0 - S$, and $H$ + LE from 16 July to 15 September 2012. The EBR was not meaningful during the morning and evening transition periods when the mean value of $R_n - G_0 - S$ was close to zero. The EBRs during the night (0000–0800 and 1900–2330) exhibited rather large or small values and are not shown in Fig. 2. The EBR pattern presented a general increase from morning to afternoon. This pattern was observed at all sites (not shown) and was also found in the FLUXNET sites in both warm and cold seasons (Wilson et al. 2002). As shown in Fig. 2, the EBR increased rapidly after 1530 and was greater than 1 by 1630, an increasing trend that continued throughout the day. The impact of wave phase difference differences in each energy balance component may be one reason for this contribution to the EBR (Gao et al. 2010). Furthermore, 19 sites were located in the oasis, and three datasets were collected in the surrounding desert. A special phenomenon known as the ''oasis effect'' was observed in the oasis. The sensible heat flux was small and even negative in the midafternoon when the sensible heat was transferred downward (stable stratification). The latent heat flux was quite large and sometimes exceeded the net radiation during the day (Fig. 9). This feature was distinctly observed on clear days in summer (Wang 1999; Liu et al. 2011) and was also reflected in diurnal behavior of the EBR.

### 2) THE INTEGRAL EBR UNDER VEGETATION SURFACES IN THE OASIS

In the kernel experimental area, there were 16 sites over vegetation surfaces. To investigate the average and integral EBR of the vegetation surfaces in the oasis, each component of the energy budget ($R_n$, $G_0$, $H$, and LE) for 16 EC sites was synchronously averaged, and the available energy against turbulent fluxes ($H$ + LE) was plotted in Fig. 3. The ratio of the turbulent energy flux to available energy was 87%, with a strong coefficient of determination (0.95). This provided an overall concept of the energy budget in the oasis. Because the canopy and photosynthesis storage measurements were not conducted for the whole experimental period, they were

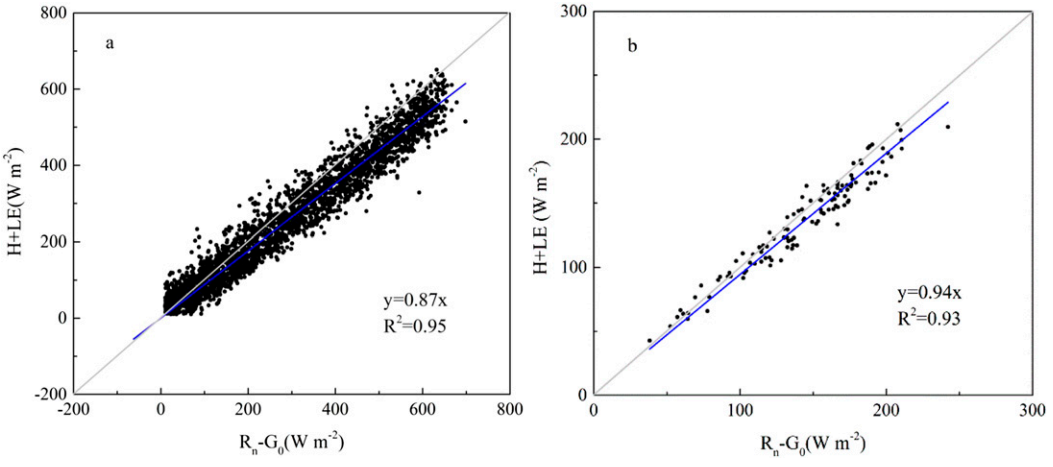


FIG. 3. Relationships (including equations and $R^2$) between the turbulent flux $H$ + LE and available energy ($x$ axis) in the kernel experimental area (16 EC sites averaged): (a) 30-min averages and (b) daily averages (June–September 2012).

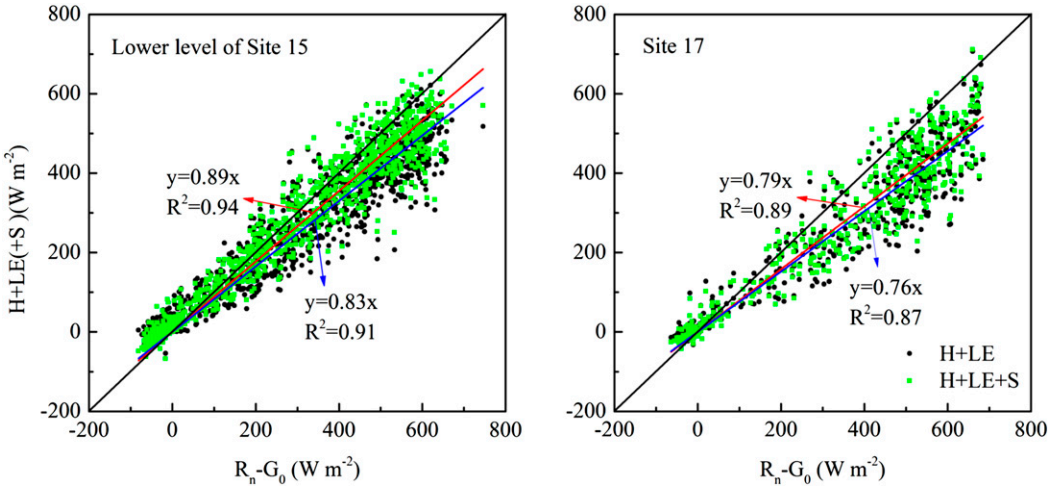


FIG. 4. Scattergram of the 30-min averages of the available energy vs the convective terms before and after correction for canopy and photosynthetic energy. The red and blue lines are the regression lines for before and after correction, respectively. (left) Site 15: 16 Jul–15 Sep 2012 and (right) site 17: 22 Aug–17 Sep 2012).

not considered in Fig. 3a. If the canopy and photosynthesis storages were considered, it is expected the energy balance closure would be enhanced by 6% (Fig. 4). The daily average energy budget component was also investigated (Fig. 3b). The storage term and the influence of phase mismatch between each energy budget component can be ignored in the daily EBR investigation. As expected, the regression slope was 0.94 with a coefficient of determination of 0.93. The analysis also indicated that the storage term cannot be ignored in the 30-min energy budget analysis and confirmed that the storage calculation was reliable.

### *b. Reasons for the energy imbalance*

Measurement errors are always mentioned as a reason for the energy imbalance of EC (e.g., Foken 2008; Cava et al. 2008), that is, underestimation of the turbulent fluxes and overestimation of net radiation. All ECs and net radiometers were compared in the Gobi Desert before the HiWATER-MUSOEXE campaign, and their high accuracy was confirmed in this study. The root-mean-square errors (RMSEs) for the EC ($H$ and LE) and net radiation ($R_n$) were 10 and 4 $W m^{-2}$ and 13 $W m^{-2}$ (systematic error), respectively (Xu et al. 2013); the uncertainties (random error) of $H$ and LE were approximately 18% and 16%, respectively (Wang et al. 2015). Furthermore, the observed data were carefully processed and rigorously screened. Because the soil heat plates were buried under the surface soil of the irrigated field, the measurements may be impacted when irrigation was applied. However, the magnitude of the soil heat flux was relatively small, especially in the long-term measurements. Therefore, instrument errors were not the main reason for the energy imbalance.

The storage terms are another potential reason for the energy imbalance. To obtain a better insight into the importance of the various storage terms, the soil heat storage, canopy storage, and photosynthesis storage were calculated separately. The soil heat storage is considered in Table 1, and the canopy and photosynthesis storage values are the focus of the following analysis. The convective terms before and after correction for canopy and photosynthetic energy are compared in Fig. 4, and site 15 (maize) and site 17 (orchard) were selected for analysis. The linear regression forced through the origin produced the equations: $y = 0.83x$ (lower level of site 15) and $y = 0.76x$ (site 17) with high coefficients of determination. When the canopy and photosynthetic energy was corrected, the linear regression slopes increased by approximately 6% and 3% at sites 15 (lower level) and 17, respectively. The percentages for the canopy and photosynthetic energy were similar and nearly equal to each other. After considering all the storage terms, the EBR at site 15 (lower level) increased from 0.87 to 0.92 during 16 July–15 September 2012, and the EBR value increased from 0.77 to 0.80 at site 17 during 22 August–17 September. The orchard area was relatively sparse when compared with the maize cropland. Thus, the canopy storage terms at site 17 were smaller than those at site 15.

Another important reason for energy imbalance was the different measurement scales of the energy balance components. During the HiWATER-MUSOEXE period, several aspects were considered in the selection of

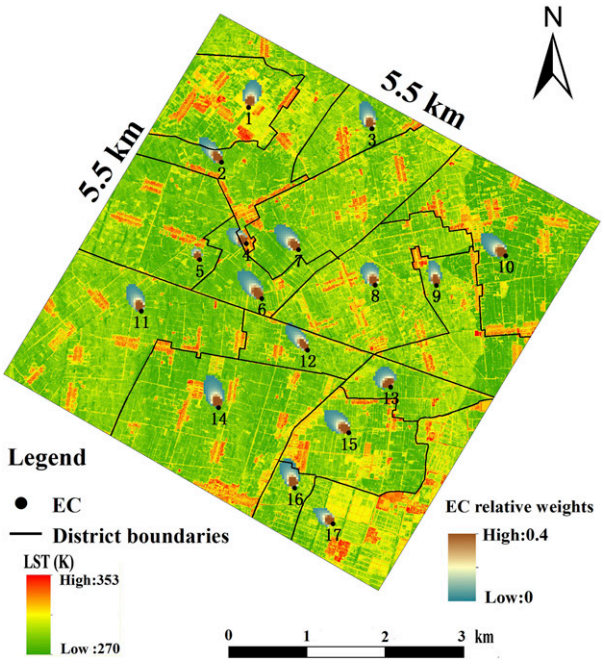


FIG. 5. The source area of EC (95% flux contribution) in each plot of the surface temperature retrieved from the TASI image on 7 Jul 2012 (passing time: 1215; resolution: 3 m).

the site locations. First, each site was chosen to be representative as much as possible (e.g., flat, homogeneous, or one type of crop). The installation heights of the EC and radiometers at each site were designed according to the size of each plot and the footprint/field of view of each instrument. The EC footprint was less than the area of its located site, and the instrument was installed at the center (Fig. 5). The primary concern was to ensure that the measurements represented the ''true'' conditions at each site. Therefore, the mismatch of measurement scales was one cause of the energy imbalance but it was not the main cause.

The experiment was performed in an oasis–desert area (30 km × 30 km) and in irrigated cropland (5.5 km × 5.5 km). The water and heat conditions and complex land surfaces affect the energy budget distribution. The following sections focus on analyzing the factors that influence the EBR in this unique study area.

### 1) THE EFFECTS OF SURFACE HETEROGENEITY

To quantify the spatial heterogeneity of the water and heat conditions in the study area, the TASI image was used. Validation showed that the accuracy of the estimated LST was better than 1.5 K (Wang et al. 2011). The source area (95% flux contribution) of 17 ECs was overlapped with the high-resolution remote sensing image in the 5.5 km × 5.5 km area (Fig. 5) using the method proposed by Kormann and Meixner (2001). The source areas of most ECs faced northwest. However, the scope of the EC source area was different distributing with different underlying surfaces and various water and heat conditions.

The seasonal variation of the averaged energy budget components ($R_n$, $G_0$, $H$, and LE at the 16 sites with vegetation surfaces) were plotted in Fig. 6 along with the estimation of the daily averaged LE based on the revised SEBS model using nine ASTER images. As can be seen, $R_n$ and LE were positive throughout the vegetation growing season, and they had the same magnitude. The values of $H$ and $G_0$ were relatively small with positive or negative values; $H$ underwent small changes from June to August and increased significantly beginning in early September, with LE decreasing at the same time because of plant wilting and the occurrence of frost. The standard deviation (SD) of $R_n$ was small, which indicated a small difference among sites. However, LE exhibited large SD, which indicated that the latent heat flux differed between sites even for the same underlying surfaces. The SEBS estimations were consistent with the ground measurements (regression slope: 3%; $R^2 = 0.66$; RMSE = 21 W m$^{-2}$), and the estimations had relatively small SD. These results indicated that the SEBS model produced good estimations; on the other hand, the SEBS model could not produce accurate estimations at every site given such heterogeneous conditions. The crop growth and irrigation amount/time (soil moisture) were different in each plot; therefore, the heterogeneity of the water and heat conditions resulted in the LE exhibiting relative large discrete values. This also resulted in the different value and variation of EBR at each site.

The experimental area (5.5 km × 5.5 km) in the irrigated cropland included 16 sites. When irrigation occurred at a site, the in situ soil water content greatly increased (inducing a difference in the soil water content and increasing surface heterogeneity) and afterward gradually spread (increasing homogeneity). Five typical sites with maize surfaces were selected, and the variations of the daily EBR and irrigation dates are shown in Fig. 7. As observed, the EBR varied daily, and it decreased during irrigation and increased after irrigation as the surface became relatively uniform.

The above analysis shows that the EBR was influenced by surface heterogeneity, and LST can provide a good indication of the degree of heterogeneity (Hoedjes et al. 2007; Liu et al. 2011). Figure 8 shows the variation of EBR at the time of the ASTER overpass versus LST in the EC source area at each site. The variation of EBR at the time of the ASTER overpass showed a declining trend as the variance of LST increasing. These results agree with the study of Stoy et al. (2013) who investigated 173 ecosystems in the FLUXNET database

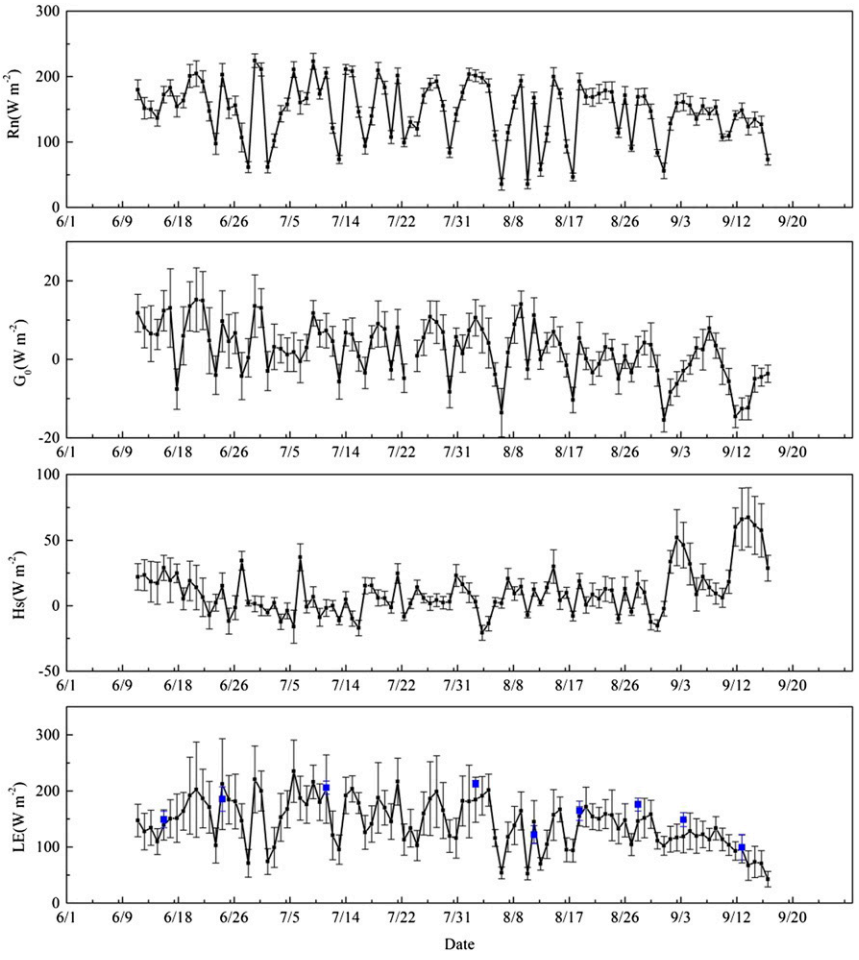


FIG. 6. The seasonal variation of the daily averaged energy budget components for vegetation surfaces. The blue rectangles in the LE panel are the estimation from the revised SEBS model of the ASTER image, and the error bars are the standard deviations.

and found that the EBR was influenced by landscape-level heterogeneity.

Therefore, we can conclude that both the variance in EBR between each plot and the energy imbalance at each site were influenced by the surface heterogeneity. The surface heterogeneity impacted the energy balance closure and may have partially resulted in advection or secondary circulations, which often emerged as organized larger eddies (Foken et al. 2010; Stoy et al. 2013). This energy might not be captured by one single EC system resulting in the energy imbalance.

2) PRELIMINARY ANALYSIS OF THE ADVECTION EFFECTS

The experimental area was located in a typical oasis–desert ecosystem. As described above, the oasis effect was observed at the superstation. This effect was observed at all the cropland sites, and we considered it an indication of a strong influence of heat advection. The result was similar to the findings of De Bruin et al. (2005). Their study was conducted in well-irrigated fields covered with alfalfa, and they reported that the correlation coefficient of air temperature and specific humidity ($R_{Tq}$) was a good indicator of the advection conditions. Typical cloudy and sunny days were selected (3 July and 3 August, respectively) and are shown in Fig. 9. As depicted, LE could significantly exceed the available energy in the afternoon if there was medium wind, especially on cloudy days. Meanwhile, $H$ was negative, LE was positive, and the indicator $R_{Tq}$ approached $-1$. In the forenoon under non-advection conditions during the day, both $H$ and LE were positive and $R_{Tq}$ was close to 1. The EBR was approximately 0.8 in the forenoon and gradually increased in the afternoon under advection conditions.

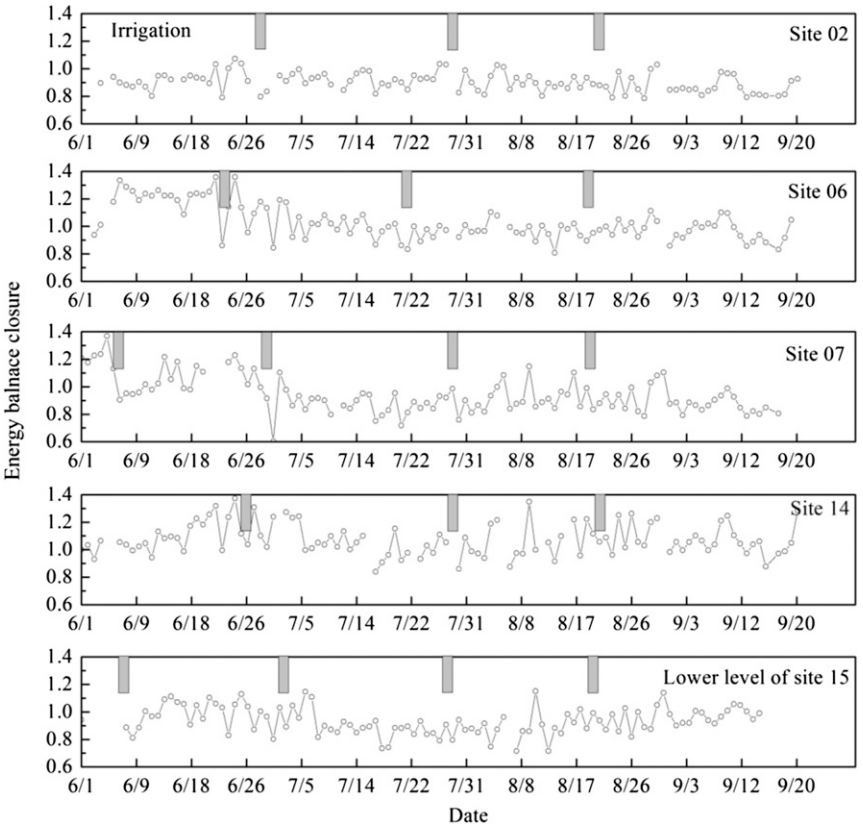


FIG. 7. The seasonal variation of the daily EBR at typical sites.

We also investigated the energy budget of a typical site (lower level of site 15) during the whole growing season by dividing the dataset based on three conditions: the whole dataset in the daytime (0700–1800 BST), data under no-advection conditions ($H > 10\,\mathrm{W\,m^{-2}}$ and 0700–1800), and data under advection conditions ($H < -10\,\mathrm{W\,m^{-2}}$ and 0700–1800). Because the observation scale of the EC system is relatively small, the averaging period should be prolonged to measure the contributions of large eddies (Finnigan et al. 2003). In each condition, the averaging period was set to 30 min, 1 h, and 2 h; meanwhile, the LAS observations of site 15 located in the pathlength (LAS4) were also plotted (Fig. 10). All three sets of conditions showed good coefficients of determination, and the EBR increased with increasing averaging period under the no-advection conditions. Under the advection conditions, the EBR was maintained at the maximum value, and it did not change with increasing averaging period. These results indicate that the energy budget should be balanced in a closed system under ideal conditions; however, advection destroys this balance by introducing extra energy (Eder et al. 2015). Other sites also showed the same phenomena (not shown), for example, site 14 with an EBR larger than 1 (Table 1) and the regression slope reached 1.10 under advection conditions. In addition, a prolonged averaging period can increase the EBR under no-advection conditions; however, uncertainty was increased because the long averaging time results in

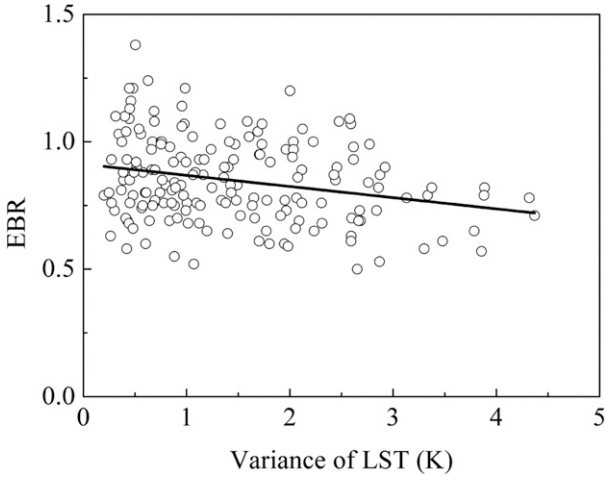


Fig. 8. The variation of EBR with the variance of the land surface temperature. Nine ASTER images retrieved the LST at each site, with a satellite passing time of 1215.

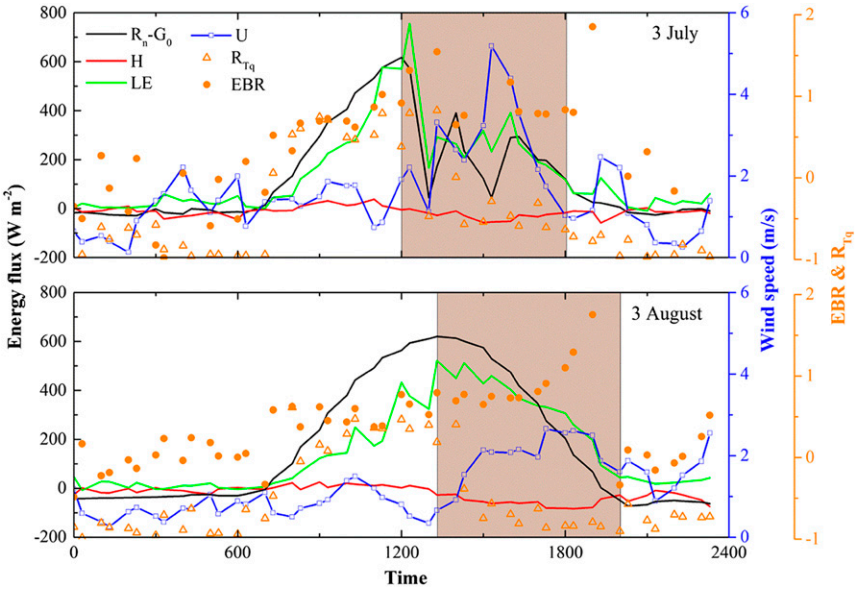


FIG. 9. Energy budget components on advective days. The brown area is the approximate period of advection (lower level of site 15).

nonstationarity. If we used the sensible heat flux measured by LAS instead of EC measurements, there were similar trends under the three conditions. However, the EBR was better than when using EC measurements. The LAS observations might be able to close the surface energy balance better than the EC method (Foken et al. 2010; Liu et al. 2011). An indicator of the correlation coefficient between vertical wind velocity and air temperature ($r_{wT}$) proposed by von Randow et al. (2006) can be used to represent the importance of low-frequency motions in the surface layer, because low-frequency processes tend to cause $r_{wT}$ to decrease. In Fig. 11, the EBR was plotted against $r_{wT}$ under no-advection conditions. The results show that the closure improved as $r_{wT}$ increased, indicating that low-frequency motions played an important role in the energy imbalance.

The cause of the energy imbalance in EC measurements is a complex issue. However, the effects of land surface heterogeneity and advection were identified as main factors of the imbalance in our experiment. The EBR decreased with heterogeneity increasing, and EBR increased when advection occurred.

## 4. Summary and conclusions

Energy imbalance is still an important issue for flux observations, and no studies have reported full energy balance closure. This study presents an analysis of the energy balance closure during the HiWATER-MUSOEXE study period, which included an intensive flux observation matrix in an oasis–desert area. An average EBR of 0.92 was obtained using the entire 30-min dataset from 22 EC sets. This provided an overall impression of EBR in the oasis–desert area of western China, which has been the subject of intensive study.

Generally, soil heat storage must be considered, and the heat storage terms (canopy and photosynthesis storage) in the energy budget improved the total closure of the maize surface by approximately 6%, demonstrating the importance of considering the heat storage of the vegetation surface. The reasons for the energy imbalance were investigated via a combination of remote sensing data and ground measurements, and we found that the land surface heterogeneity level had a significant influence on the EBR. The EBR decreased with land surface heterogeneity increasing (e.g., during irrigation) in almost all EC sets in the flux matrix. This was related to the larger eddies because the EBR increased with longer averaging periods (e.g., from 30 min to 2 h), which can capture more eddies. Strong advection or secondary circulation usually occurred during the afternoon in the experimental area, which broke the closed system of the energy balance and caused an increasing EBR trend during the day.

Although the issue of the lack of energy balance closure is still under debate, many researchers have deemed it a scale problem; that is, EC measurements at a single station cannot capture the energy flux from larger eddies and secondary circulations (Foken 2008; Foken et al. 2010, 2011). A similar result was found in

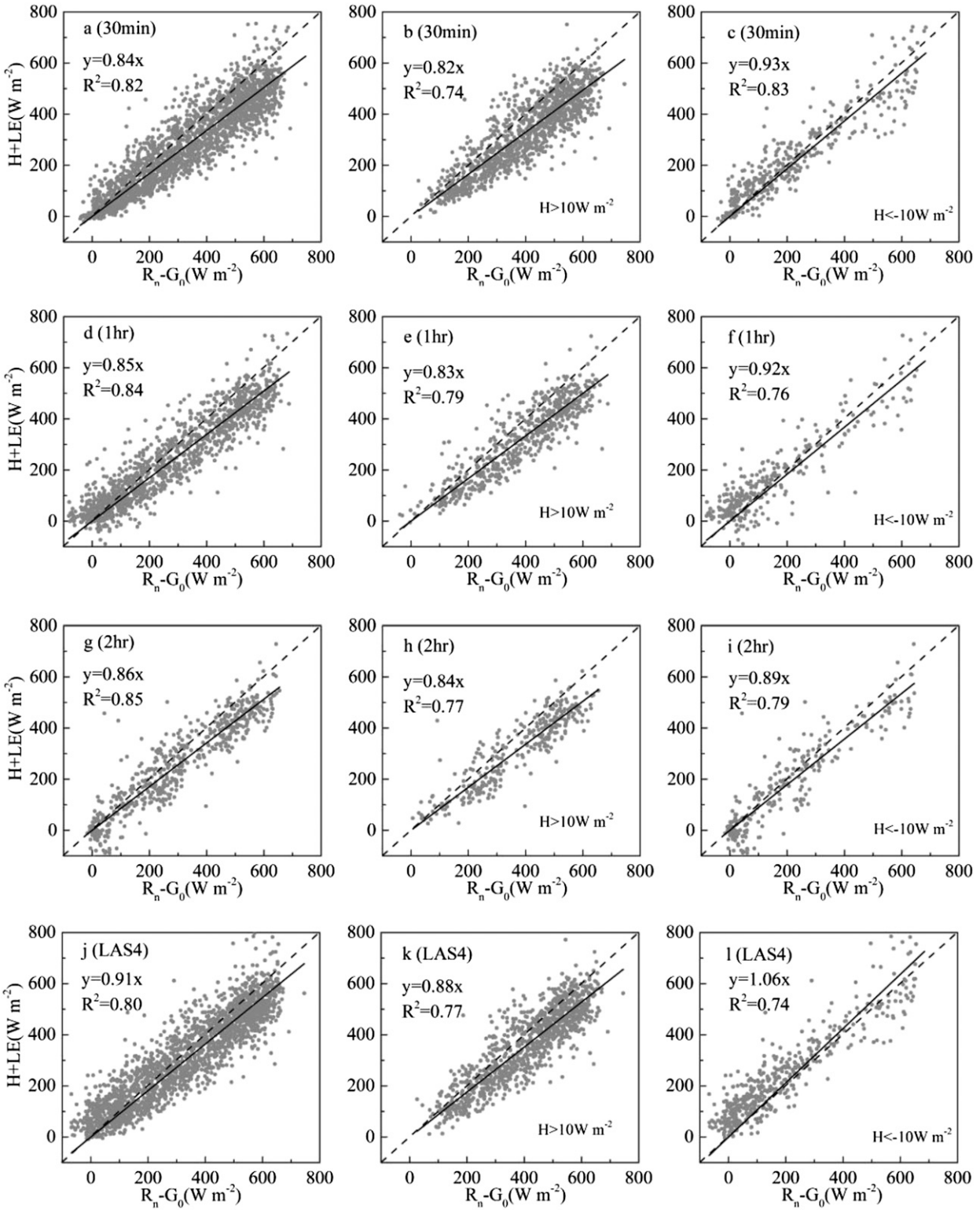


FIG. 10. The sum of $H$ and LE vs the available energy averaged every 30 min, 1 h, and 2 h, as well as the LAS observations during the day. The three columns represent (left) the whole dataset, (center) under no-advection conditions ($H > 10\,\mathrm{W\,m^{-2}}$), and (right) under advection conditions ($H < -10\,\mathrm{W\,m^{-2}}$) at the lower level of site 15 during 0700–1800 BST.

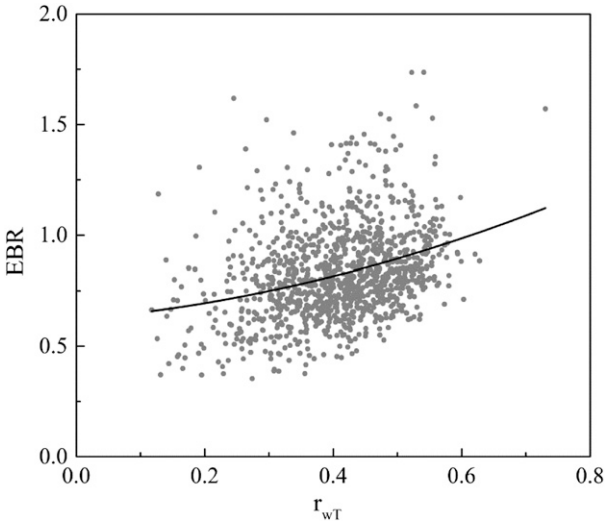


FIG. 11. The variation of EBR with the coefficient of vertical velocity and temperature (lower level of site15, $H > 10$ W m$^{-2}$, and 0700–1800).

the present study; surface heterogeneity may result in large eddies or organized coherent structures. The quantitative explanations behind the relationships between EBR and both surface heterogeneity and advection should be investigated mechanistically in future studies.

*Acknowledgments.* We thank all the scientists, engineers, and students who participated in HiWATER field campaigns. This work was supported by National Science Foundation of China (41301355), the National Basic Research Program of China (2015CB953702), and the National Science Foundation of China (41371002, 41271345).

## REFERENCES

Aubinet, M., and Coauthors, 2000: Estimates of the annual net carbon and water exchange of European forest: The EUROFLUX methodology. *Adv. Ecol. Res.*, **30**, 114–175.

——, T. Vesala, and D. Papale, 2012: *Eddy Covariance: A Practical Guide to Measurement and Data Analysis.* Springer, 438 pp.

Bai, J., L. Jia, S. M. Liu, Z. W. Xu, G. C. Hu, M. J. Zhu, and L. S. Song, 2015: Characterizing the footprint of eddy covariance system and large aperture scintillometer measurements to validate satellite-based surface fluxes. *IEEE Geosci. Remote Sens. Lett.*, **12**, 943–947, doi:10.1109/LGRS.2014.2368580.

Berbigier, P., J. M. Bonnefond, and P. Mellmann, 2001: $CO_2$ and water vapour fluxes for 2 years above Euroflux forest site. *Agric. For. Meteor.*, **108**, 183–197, doi:10.1016/S0168-1923(01)00240-4.

Beyrich, F., H. A. R. Debruin, and W. M. L. Meijninger, 2002: Results from one-year continuous operation of a large aperture scintillometer over a heterogeneous land surface. *Bound.-Layer Meteor.*, **105**, 85–97, doi:10.1023/A:1019640014027.

Cava, D., D. Contini, A. Donateo, and P. Martano, 2008: Analysis of short-term closure of the surface energy balance above short vegetation. *Agric. For. Meteor.*, **148**, 82–93, doi:10.1016/j.agrformet.2007.09.003.

De Bruin, H. A. R., O. K. Hartogensis, R. G. Allen, and J. W. J. L. Kramer, 2005: Regional Advection Perturbations in an Irrigated Desert (RAPID) experiment. *Theor. Appl. Climatol.*, **80**, 143–152, doi:10.1007/s00704-004-0096-x.

Eder, F., F. De Roo, E. Rotenberg, D. Yakir, H. P. Schmid, and M. Mauder, 2015: Secondary circulations at a solitary forest surrounded by semi-arid shrubland and their impact on eddy-covariance measurements. *Agric. For. Meteor.*, **211–212**, 115–127, doi:10.1016/j.agrformet.2015.06.001.

Fang, C., and J. B. Moncrieff, 2001: The dependence of soil $CO_2$ efflux on temperature. *Soil Biol. Biochem.*, **33**, 155–165, doi:10.1016/S0038-0717(00)00125-5.

Finnigan, J. J., R. Clement, Y. Malhi, R. Leuning, and A. Cleugh, 2003: A re-evaluation of long-term flux measurement techniques, Part I: Averaging and coordinate rotation. *Bound.-Layer Meteor.*, **107**, 1–48, doi:10.1023/A:1021554900225.

Foken, T., 2008: The energy balance closure problem—An overview. *Ecol. Appl.*, **18**, 1351–1367, doi:10.1890/06-0922.1.

——, and Coauthors, 2010: Energy balance closure for the LITFASS-2003 experiment. *Theor. Appl. Climatol.*, **101**, 149–160, doi:10.1007/s00704-009-0216-8.

——, M. Aubinet, J. J. Finnigan, M. Y. Leclerc, M. Mauder, and K. T. Paw, 2011: Results of a panel discussion about the energy balance closure correction for trace gases. *Bull. Amer. Meteor. Soc.*, **92**, ES13–ES18, doi:10.1175/2011BAMS3130.1.

Franssen, H. J. H., R. Stöckli, I. Lehner, E. Rotenberg, and S. I. Seneviratne, 2010: Energy balance closure of eddy-covariance dada: A multisite analysis for European FLUXNET stations. *Agric. For. Meteor.*, **150**, 1553–1567, doi:10.1016/j.agrformet.2010.08.005.

Gao, Z., R. Horton, and H. P. Liu, 2010: Impact of wave phase difference between soil surface heat flux and soil surface temperature on soil surface energy balance closure. *J. Geophys. Res.*, **115**, D16112, doi:10.1029/2009JD013278.

Hoedjes, J. C. B., A. Chehbouni, J. Ezzahar, R. Escadafal, and H. A. R. De Bruin, 2007: Comparison of large aperture scintillometer and eddy covariance measurements: Can thermal infrared data be used to capture footprint-induced differences? *J. Hydrometeor.*, **8**, 144–159, doi:10.1175/JHM561.1.

Jacobs, A. F. G., B. G. Heusinkveld, and A. A. M. Holtslag, 2003: Carbon dioxide and water vapour flux densities over a grassland area in The Netherlands. *Int. J. Climatol.*, **23**, 1663–1675, doi:10.1002/joc.959.

——, ——, and ——, 2008: Towards closing the surface energy budget of a mid-latitude grassland. *Bound.-Layer Meteor.*, **126**, 125–136, doi:10.1007/s10546-007-9209-2.

Jia, Z. Z., S. M. Liu, Z. W. Xu, Y. J. Chen, and M. J. Zhu, 2012: Validation of remotely sensed evapotranspiration over the Hai River basin, China. *J. Geophys. Res.*, **117**, D13113, doi:10.1029/2011JD017037.

Kanemasu, E. T., and Coauthors, 1992: Surface flux measurements in FIFE: An overview. *J. Geophys. Res.*, **97**, 18 547–18 555, doi:10.1029/92JD00254.

Kawai, T., and M. Kanda, 2010: Urban energy balance obtained from the comprehensive outdoor scale model experiment. Part I: Basic features of the surface energy balance. *J. Appl. Meteor. Climatol.*, **49**, 1341–1359, doi:10.1175/2010JAMC1992.1.

Kormann, R., and F. X. Meixner, 2001: An analytic footprint model for non-neutral stratification. *Bound.-Layer Meteor.*, **99**, 207–224, doi:10.1023/A:1018991015119.

Li, X., and Coauthors, 2013: Heihe Watershed Allied Telemetry Experimental Research (HiWATER): Scientific objectives and experimental design. *Bull. Amer. Meteor. Soc.*, **94**, 1145–1160, doi:10.1175/BAMS-D-12-00154.1.

Li, Z., G. Yu, X. Wen, L. Zhang, C. Ren, and Y. Fu, 2005: Energy balance closure at ChinaFLUX sites. *Sci. China*, **48D**, 51–62.

Liebethal, C., B. Huwe, and T. Foken, 2005: Sensitivity analysis for two ground heat flux calculation approaches. *Agric. For. Meteor.*, **132**, 253–262, doi:10.1016/j.agrformet.2005.08.001.

Liu, S. M., Z. W. Xu, W. Z. Wang, Z. Z. Jia, M. J. Zhu, and J. M. Wang, 2011: A comparison of eddy-covariance and large aperture scintillometer measurements with respect to the energy balance closure problem. *Hydrol. Earth Syst. Sci.*, **15**, 1291–1306, doi:10.5194/hess-15-1291-2011.

——, ——, Z. L. Zhu, Z. Z. Jia, and M. J. Zhu, 2013: Measurements of evapotranspiration from eddy-covariance systems and large aperture scintillometers in the Hai River basin, China. *J. Hydrol.*, **487**, 24–38, doi:10.1016/j.jhydrol.2013.02.025.

——, and Coauthors, 2016: Upscaling multi-site measurements over heterogeneous land surfaces for surface evapotranspiration at satellite pixel scale. *Agric. For. Meteor.*, **230–231**, 97–113, doi:10.1016/j.agrformet.2016.04.008.

Ma, Y. F., S. M. Liu, F. Zhang, J. Zhou, and Z. Z. Jia, 2015: Estimations of regional surface energy fluxes over heterogeneous oasis–desert surfaces in the middle reaches of the Heihe River during HiWATER-MUSOEXE. *IEEE Geosci. Remote Sens. Lett.*, **12**, 671–675, doi:10.1109/LGRS.2014.2356652.

Mauder, M., and T. Foken, 2004: Documentation and instruction manual of the eddy covariance software package TK2. Department of Micrometeorology, University of Bayreuth Rep. 26, 44 pp.

——, C. Liebethal, M. Göckede, J.-P. Leps, F. Beyrich, and T. Foken, 2006: Processing and quality control of flux data during LITFASS-2003. *Bound.-Layer Meteor.*, **121**, 67–88, doi:10.1007/s10546-006-9094-0.

Meyers, T. P., and S. E. Hollinger, 2004: An assessment of storage terms in the surface energy balance of maize and soybean. *Agric. For. Meteor.*, **125**, 105–115, doi:10.1016/j.agrformet.2004.03.001.

Oncley, S. P., and Coauthors, 2007: The energy balance experiment EBEX-2000. Part I: Overview and energy balance. *Bound.-Layer Meteor.*, **123**, 1–28, doi:10.1007/s10546-007-9161-1.

Panin, G. N., G. Tetzlaff, and A. Raabe, 1998: Inhomogeneity of the land surface and problems in the parameterization of surface fluxes in natural conditions. *Theor. Appl. Climatol.*, **60**, 163–178, doi:10.1007/s007040050041.

Sánchez, J. M., V. Caselles, and E. M. Rubio, 2010: Analysis of the energy balance closure over a FLUXNET boreal forest in Finland. *Hydrol. Earth Syst. Sci.*, **14**, 1487–1497, doi:10.5194/hess-14-1487-2010.

Stoy, P. C., and Coauthors, 2013: A data-driven analysis of energy balance closure across FLUXNET research sites: The role of landscape scale heterogeneity. *Agric. For. Meteor.*, **171–172**, 137–152, doi:10.1016/j.agrformet.2012.11.004.

Su, Z., 2002: The Surface Energy Balance System (SEBS) for estimation of turbulent heat fluxes. *Hydrol. Earth Syst. Sci.*, **6**, 85–100, doi:10.5194/hess-6-85-2002.

Tsvang, L. R., M. M. Fedorov, B. A. Kader, S. L. Zubkovskii, T. Foken, S. H. Richter, and Y. A. Zeleny, 1991: Turbulent exchange over a surface with chessboard-type inhomogeneities. *Bound.-Layer Meteor.*, **55**, 141–160, doi:10.1007/BF00119331.

Twine, T. E., and Coauthors, 2000: Correcting eddy-covariance flux underestimates over a grassland. *Agric. For. Meteor.*, **103**, 279–300, doi:10.1016/S0168-1923(00)00123-4.

Von Randow, C., B. Kruijt, and A. A. M. Holtslag, 2006: Low-frequency modulation of the atmospheric surface layer over Amazonian rain forest and its implication for similarity relationships. *Agric. For. Meteor.*, **141**, 192–207, doi:10.1016/j.agrformet.2006.10.005.

Wang, H., Q. Xiao, H. Li, and B. Zhong, 2011: Temperature and emissivity separation algorithm for TASI airborne thermal hyperspectral data. *Proc. IEEE Int. Geoscience and Remote Sensing Symp.*, Vancouver, BC, Canada, IEEE, 1075–1078, doi:10.1109/ICECC.2011.6066288.

Wang, J. M., 1999: Land surface process experiments and interaction study in China—From HEIFE to IMGRASS and GAME Tibet/TIPEX (in Chinese with English abstract). *Plateau Meteor.*, **18**, 280–294.

——, J. X. Zhuang, W. Z. Wang, S. M. Liu, and Z. W. Xu, 2015: Assessment of uncertainties in eddy covariance flux measurement based on intensive flux matrix of HiWATER-MUSOEXE. *IEEE Geosci. Remote Sens. Lett.*, **12**, 259–263, doi:10.1109/LGRS.2014.2334703.

Wang, W. Z., Y. S. Huang, F. Y. Xu, C. F. Ma, and J. Wang, 2012: HiWATER: Dataset of biomass observed in the middle reaches of the Heihe River basin. Cold and Arid Regions Environmental and Engineering Research Institute, Chinese Academy of Sciences, doi:10.3972/hiwater.122.2013.db.

Wilson, K., and Coauthors, 2002: Energy balance closure at FLUXNET sites. *Agric. For. Meteor.*, **113**, 223–243, doi:10.1016/S0168-1923(02)00109-0.

Xu, T. R., S. M. Liu, S. L. Liang, and J. Qin, 2011: Improving predictions of water and heat fluxes by assimilating MODIS land surface temperature products into the Common Land Model. *J. Hydrometeor.*, **12**, 227–244, doi:10.1175/2010JHM1300.1.

——, ——, L. Xu, Y. J. Chen, Z. Z. Jia, Z. W. Xu, and J. Nielson, 2015: Temporal upscaling and reconstruction of thermal remotely sensed instantaneous evapotranspiration. *Remote Sens.*, **7**, 3400–3425, doi:10.3390/rs70303400.

Xu, Z. W., and Coauthors, 2013: Intercomparison of surface energy flux measurement systems used during the HiWATER-MUSOEXE. *J. Geophys. Res. Atmos.*, **118**, 13 140–13 157, doi:10.1002/2013JD020260.

Yang, K., and J. M. Wang, 2008: A temperature prediction-correction method for estimating surface soil heat flux from soil temperature and moisture data. *Sci. China*, **51D**, 721–729, doi:10.1007/s11430-008-0036-1.

Zhou, J., M. S. Li, S. M. Liu, Z. Z. Jia, and Y. F. Ma, 2015: Validation and performance evaluations of methods for estimating land surface temperatures from ASTER data in the middle reach of the Heihe River basin, northwest China. *Remote Sens.*, **7**, 7126–7156, doi:10.3390/rs70607126.